

Super Realized Gain Antenna Array

Dónal Patrick Lynch¹, *Graduate Student Member, IEEE*, Manos M. Tentzeris², *Fellow, IEEE*,
Vincent Fusco¹, *Fellow, IEEE*, and Stylianos D. Asimonis¹, *Senior Member, IEEE*

Abstract—In this study, we introduce a novel antenna design method for superdirective antennas that combines low complexity with high radiation efficiency, while being impedance-matched to 50 Ω . We applied this approach to design, fabricate, and measure a superdirective antenna array (SDA) with a high realized antenna gain (i.e., 6.3 dBi) and radiation efficiency (i.e., 99.3%), consisting of two strip dipole elements operating at a frequency of 3.5 GHz. The fabricated antenna has an electrical size of 1.55, underscoring its compactness in addition to its high gain. Our approach is distinguished by its ability to achieve high directivity and radiation efficiency, along with impedance-matching to 50 Ω , through meticulous adjustments of the strip dimensions (i.e., length and width) and the phase difference between elements. This method eliminates the need for external impedance-matching networks, amplifiers, attenuators, parasitic elements, or loads, marking a significant advancement in the development of practical superdirective antenna designs.

Index Terms—Antenna arrays, antennas, dipole antennas, directive antennas, microstrip antenna arrays, superdirective antenna arrays (SDAs).

I. INTRODUCTION

THE advent of modern mobile communication networks, including fifth-generation (5G), sixth-generation (6G), and beyond, has been driven by the ever-increasing demand for faster download speeds and low latency, enabling seamless connectivity to work and social digital platforms. With the exponential growth of data-intensive applications and the need for reliable connectivity, these systems have become a necessary response to meet the evolving requirements of today's digital society. One of the critical aspects of these advanced communication technologies is the deployment of efficient and advanced antenna systems [1], [2] to support the enhanced capabilities of these networks.

In the context of 5G [3], which is currently the most prevalent mobile communication technology, the frequency band most widely used for applications falls within the range of 3.3–4.2 GHz. The selection of the sub-6 GHz range for 5G deployment is driven by the desire to strike a balance between coverage and capacity. However, the transition to 5G communication systems requires the use of high-gain antennas

to compensate for the higher path losses associated with higher frequency operation. This results in antennas that are not only larger in size but also more complex in geometry. Such an escalation in both the dimensions and complexity presents significant challenges to antenna design. This complexity also contributes to an increase in manufacturing costs. It is therefore crucial to use sophisticated antenna design techniques to simultaneously achieve high gain and maintain compactness, facilitating the seamless integration of 5G antenna systems into diverse applications without compromising performance.

To address the challenges posed by the large size and high-gain requirements of 5G antenna systems, researchers are exploring innovative approaches, with superdirective antenna arrays (SDAs) emerging as a particularly promising solution. The concept of superdirectivity was first introduced by Uskov [4], who demonstrated through theoretical analysis that a uniform linear array (ULA) of N isotropic radiators can achieve endfire directivity approaching N^2 as the spacing between elements approaches zero, assuming the radiators are excited with appropriately chosen voltage signals. Hansen further refined the concept of superdirectivity by establishing a criterion for SDAs: an array is considered superdirective if its directivity surpasses that of an identical array with uniform excitation [5]. This principle enables SDAs to maintain compact designs while achieving higher directivity than traditional antenna arrays. Subsequent studies have focused on analyzing and developing SDAs [6], [7], [8], [9], [10], [11], [12], [13], [14], [15], [16], [17], [18], [19], [20], with many attempting to link superdirectivity with Harrington's theoretical maximum directivity limit, which is $M^2 + 2M$ and depends on the number of orthogonal modes, M , of the antenna [6]. Nonetheless, it is important to clarify that Harrington's limit is not the defining criterion for superdirectivity.

It is crucial to acknowledge that SDAs come with certain disadvantages and barriers to their practical deployment. A primary limitation is the necessity to drive the antenna with precisely selected voltage signals, implying the need for amplifiers or attenuators. This requirement not only increases the complexity of the antenna system but also escalates the ohmic losses. These losses, in turn, reduce the radiation efficiency and thus the antenna gain. In addition, the impedance characteristics of SDA elements often exhibit high reactance, making it challenging to achieve impedance-matching at the standard 50 Ω [21], thus complicating the practical implementation of superdirective arrays.

To address these limitations, researchers have suggested incorporating parasitic elements and/or additional loads strategically positioned on the radiating elements of the antenna array, as demonstrated in various studies [22], [23], [24], [25], [26]. Although these methods can reduce high losses, they often result in complex antenna designs. Moreover, many of these approaches do not adequately consider

Manuscript received 28 March 2024; revised 18 June 2024; accepted 23 July 2024. Date of publication 7 August 2024; date of current version 9 September 2024. This work was supported by the Department for the Economy (DfE), Northern Ireland. (*Corresponding author: Dónal Patrick Lynch.*)

Dónal Patrick Lynch, Vincent Fusco, and Stylianos D. Asimonis are with the Centre for Wireless Innovation (CWI), ECIT Institute, Queen's University Belfast, BT3 9DT Belfast, U.K. (e-mail: dlynch27@qub.ac.uk; v.fusco@ecit.qub.ac.uk; s.asimonis@qub.ac.uk).

Manos M. Tentzeris is with the School of Electrical and Computer Engineering, Georgia Institute of Technology, Atlanta, GA 30332 USA (e-mail: etentze@ece.gatech.edu).

Color versions of one or more figures in this article are available at <https://doi.org/10.1109/TAP.2024.3437218>.

Digital Object Identifier 10.1109/TAP.2024.3437218

the impact of impedance mismatch losses. A conventional method for reducing return losses involves designing an impedance-matching network for the superdirective antenna. While this strategy can effectively decrease mismatch losses, it also introduces higher ohmic losses into the system. This tradeoff underscores why antenna designs often prioritize impedance-matched antennas directly, rather than relying on additional impedance-matching networks.

Consequently, there is a pressing demand for a superdirective antenna design approach that is low in complexity, minimizes radiation losses, avoids the need for extra impedance-matching networks, and achieves impedance-matching to 50Ω directly. In addition, this design should eliminate the need to adjust the magnitude of the excitation voltage signals, thereby obviating the need for attenuators and/or amplifiers.

The contribution of our work lies in the design of a low-complexity superdirective antenna that does not require the use of amplifiers, attenuators, impedance-matching networks, loads, or parasitic elements. Our design uses only two driven dipoles, each approximately half a wavelength in length. Through theoretical analysis, simulations, and measurements, we have demonstrated that by slightly adjusting the length and width of the dipoles, we can achieve directivity very close to Harrington's theoretical limit, alongside high radiation efficiency and impedance-matching to 50Ω . Another innovative aspect of our work is that our entire development is based on the realized gain, which accounts for both ohmic and return losses. This antenna design approach, presented for the first time in the literature, represents a novel example of a low-complexity superdirective antenna.

This article is structured as follows: We first introduce our proposed antenna design approach and validate it through theoretical analysis, using analytical expressions for two adjacent linear dipoles. We corroborate our theoretical analysis with numerical analysis for additional verification. Building on these insights, we then proceed with the design of a two-element strip dipole antenna array. The resulting design undergoes comprehensive simulation via full-electromagnetic analysis, followed by fabrication and measurement of gain and return losses. The measured results closely match our simulated and theoretical predictions. Finally, the antenna is evaluated against cutting-edge designs. Contrary to the current state-of-the-art, the proposed superdirective antenna features a low profile and exhibits high radiation efficiency and directivity, closely approaching the maximum Harrington limit. In addition, it achieves impedance-matching to 50Ω .

II. ANTENNA DESIGN

A. Theoretical Analysis

When antennas are located in close proximity, the effect of mutual coupling between them cannot be ignored. The mutual impedance serves as an indicator of the degree to which antenna cross interaction proximity effects are present. This section presents the theoretical analysis of a two-element antenna array, as depicted in Fig. 1. The array consists of linear wire dipoles arranged in a parallel, side-by-side format along the ρ -axis at a distance d from each other, with centers at positions (x_i, y_i) , lengths L_i , radii a_i , input voltages, and currents V_i and I_i , respectively, where $i = 1, 2$. To evaluate the mutual and self-impedances Z_{ij} of the antenna array,

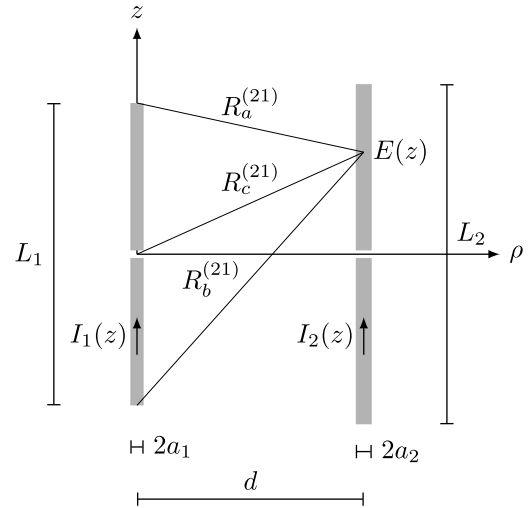


Fig. 1. Array of wire dipole antennas with an interelement distance of d , lengths of elements L_1 and L_2 , and radii of elements a_1 and a_2 .

where $i, j = 1, 2$, we consider it as a two-port network. Therefore, in general, when both the antennas are excited, the relationship between the driving voltages and input currents is expressed as follows [27]:

$$\begin{bmatrix} V_1 \\ V_2 \end{bmatrix} = \begin{bmatrix} Z_{11} & Z_{12} \\ Z_{21} & Z_{22} \end{bmatrix} \begin{bmatrix} I_1 \\ I_2 \end{bmatrix} \Leftrightarrow \mathbf{v} = \mathbf{Z}_n \mathbf{i}_n. \quad (1)$$

The impact of the first dipole on the second dipole is represented by the mutual impedance Z_{21} , which is defined as [28]

$$Z_{21} = \frac{V_2^{oc}}{I_1}. \quad (2)$$

Thus, the mutual impedance Z_{21} is defined as the ratio of the induced open-circuited voltage at the terminals of the second dipole when only the first dipole is driven, and vice versa for Z_{12} . Note that according to reciprocity, $Z_{21} = Z_{12}$. The induced open-circuited voltage is given by [28]

$$V_2^{oc} = -\frac{1}{I_2} \int_{-l_2}^{l_2} E_z(z) I_2(z) dz \quad (3)$$

where $l_2 = L_2/2$ and $E_z(z)$ is the electric field caused by the driven first dipole on the second dipole. To calculate $E_z(z)$, we need to define the currents that flow through the dipoles. We assume that the dipoles have lengths close to half-wavelength, so we can use a sinusoidal current distribution in this analysis. Thus, we have

$$I_2(z) = I_2 \frac{\sin[k(l_2 - |z|)]}{\sin[k l_2]}, \quad |z| \leq l_2 \quad (4)$$

where $I_2 \in \mathbb{C}$ is the input current of the second dipole, $k = 2\pi/\lambda$ is the wavenumber, and λ is the wavelength. Note that $I_1(z)$ can also be given by (4) by setting $I_2 \rightarrow I_1$ and $l_2 \rightarrow l_1 = L_1/2$. The electric field along the second antenna is given by [28]

$$E_z(z) = -j \frac{\eta_0 I_1}{4\pi \sin[k l_1]} \left(\frac{e^{-jkR_a^{(21)}}}{R_a^{(21)}} + \frac{e^{-jkR_b^{(21)}}}{R_b^{(21)}} - 2 \cos[k l_1] \frac{e^{-jkR_c^{(21)}}}{R_c^{(21)}} \right) \quad (5)$$

where η_0 is the characteristic impedance of free space and $z \in [-l_2, l_2]$, and

$$\begin{aligned} R_a^{(21)} &= \sqrt{d^2 + (z - l_1)^2} \\ R_b^{(21)} &= \sqrt{d^2 + (z + l_1)^2} \\ R_c^{(21)} &= \sqrt{d^2 + z^2}. \end{aligned} \quad (6)$$

By substituting (3)–(6) into (2)

$$Z_{21} = j \frac{\eta_0}{4\pi \sin[k l_1] \sin[k l_2]} \int_{-l_2}^{l_2} A_{21}(z) dz \quad (7)$$

where

$$A_{21}(z) = \left(\frac{e^{-jkR_a^{(21)}}}{R_a^{(21)}} + \frac{e^{-jkR_b^{(21)}}}{R_b^{(21)}} - 2 \cos[k l_1] \frac{e^{-jkR_c^{(21)}}}{R_c^{(21)}} \right) \sin[k(l_2 - |z|)]. \quad (8)$$

Note that the integral in (7) does not have an analytical solution. Therefore, we used numerical integration techniques, specifically global adaptive quadrature, to accurately evaluate the integral [29].

To obtain the near-field on the surface of the first dipole, we set $d \rightarrow a_1$ and $l_2 \rightarrow l_1$ in (6) because the integral is now estimated on the first dipole, and not on the second. The resulting expression is

$$Z_{11} = j \frac{\eta_0}{4\pi \sin^2[k l_1]} \int_{-l_1}^{l_1} A_{11}(z) dz \quad (9)$$

where now

$$A_{11}(z) = \left(\frac{e^{-jkR_a^{(11)}}}{R_a^{(11)}} + \frac{e^{-jkR_b^{(11)}}}{R_b^{(11)}} - 2 \cos[k l_1] \frac{e^{-jkR_c^{(11)}}}{R_c^{(11)}} \right) \sin[k(l_1 - |z|)] \quad (10)$$

and

$$\begin{aligned} R_a^{(11)} &= \sqrt{a_1^2 + (z - l_1)^2} \\ R_b^{(11)} &= \sqrt{a_1^2 + (z + l_1)^2} \\ R_c^{(11)} &= \sqrt{a_1^2 + z^2}. \end{aligned} \quad (11)$$

Similar analysis can be applied to estimate Z_{22} . With the given driven voltages \mathbf{v} , solving (1) provides the input currents \mathbf{i}_n , which are used to define the sinusoidal currents $I_i(z)$ based on (4). Thus

$$\mathbf{i}_n = \mathbf{Z}_n^{-1} \mathbf{v} \quad (12)$$

where $(\)^{-1}$ denotes the inverse matrix.

By determining the currents \mathbf{i}_n , the radiation pattern of the array can be obtained, and the radiation intensity can be expressed as

$$\begin{aligned} U(\mathbf{i}_n, \theta, \phi) &= \frac{\eta_0}{8\pi^2} \left| \sum_{i=1}^N I_i \frac{\cos[k l_i \cos \theta] - \cos[k l_i]}{\sin \theta} e^{jk \vec{d}_i} \right|^2 \end{aligned} \quad (13)$$

where N is the number of antenna array elements (in this example, $N = 2$ since we have two dipoles), $\vec{k} = k \hat{r}$ is the wavevector, where

$$\hat{r} = \sin \theta \cos \phi \hat{x} + \sin \theta \sin \phi \hat{y} + \cos \theta \hat{z} \quad (14)$$

is the unit vector in spherical coordinates, and $\vec{d}_i = x_i \hat{x} + y_i \hat{y} + z_i \hat{z}$ is the vector that indicates the position of the dipoles. Hence, the directivity is given by

$$D \triangleq 4\pi \frac{U(\mathbf{i}_n, \theta, \phi)}{P_r} \quad (15)$$

where

$$P_r \triangleq \int_{\phi=0}^{2\pi} \int_{\theta=0}^{\pi} U(\mathbf{i}_n, \theta, \phi) \sin \theta d\theta d\phi \quad (16)$$

is the total radiated power. The radiated power represents a portion of the input power to the two-port system and is defined as

$$P_{in} \triangleq P_r + P_l \quad (17)$$

where P_l represents the ohmic losses on the dipoles. In the calculation of directivity, it is assumed that there are no ohmic losses on the antenna array, and therefore all the input power is radiated. In this scenario (i.e., $P_l \rightarrow 0$), it can be presumed that $P_{in} = P_r$, as stated in [14]

$$\begin{aligned} P_r &= \frac{1}{2} \text{Re} \{ \mathbf{i}_n^H \mathbf{Z}_n \mathbf{i}_n \} \\ &= \frac{1}{2} \text{Re} \{ (\mathbf{Z}_n^{-1} \mathbf{v})^H \mathbf{v} \} \end{aligned} \quad (18)$$

where $(\)^H$ denotes the Hermitian transpose.

On the other hand, when calculating the gain of an antenna array, it is essential to consider the ohmic losses associated with the wire dipoles. In general, the gain of an antenna is given by

$$G \triangleq 4\pi \frac{U(\mathbf{i}_l, \theta, \phi)}{P_{in}} = 4\pi \frac{U(\mathbf{i}_l, \theta, \phi)}{P_r + P_l} \quad (19)$$

where now $P_l \neq 0$. Ohmic losses are a result of the *skin effect* [30]. Based on this effect, we can derive the loss resistance per unit length on the i th conductive wire dipole as

$$r_{l,i} = \frac{1}{2a_i} \sqrt{\frac{f \mu_0}{\pi \sigma}} \quad (20)$$

where f , $\mu_0 = 4\pi \times 10^{-7}$ H/m, and σ are the operating frequency, magnetic permeability of free space, and wire conductivity, respectively. Thus, for the current distribution of (4)

$$R_{l,i} = r_{l,i} \int_{-l_i}^{l_i} \left| \frac{I_i(z)}{I_i} \right|^2 dz = \frac{k L_i - \sin[k L_i]}{4ka_i \sin^2[k \frac{L_i}{2}]} \sqrt{\frac{f \mu_0}{\pi \sigma}}. \quad (21)$$

In addition, the relationship between the driving voltages and the input currents is now expressed as follows:

$$\mathbf{v} = \mathbf{Z}_l \mathbf{i}_l = (\mathbf{Z}_n + \mathbf{R}_l) \mathbf{i}_l \quad (22)$$

where $\mathbf{R}_l = \text{diag}(R_{l,1}, \dots, R_{l,N})$, and \mathbf{i}_l is the matrix of the input currents of the lossy network. Hence, similar to (12)

$$\mathbf{i}_l = (\mathbf{Z}_n + \mathbf{R}_l)^{-1} \mathbf{v}. \quad (23)$$

The input power is now given by

$$\begin{aligned} P_{in} &= \frac{1}{2} \text{Re} \{ \mathbf{i}_1^H (\mathbf{Z}_n + \mathbf{R}_1) \mathbf{i}_1 \} \\ &= \frac{1}{2} \text{Re} \left\{ ((\mathbf{Z}_n + \mathbf{R}_1)^{-1} \mathbf{v})^H \mathbf{v} \right\}. \end{aligned} \quad (24)$$

The definition of the directivity and gain of an antenna array incorporates the corresponding power density. The power density is determined by the input currents, which do not consider the ohmic losses on the radiating elements when estimating directivity, but do take into account the ohmic losses when estimating gain. Consequently, the power density for directivity (i.e., $U(\mathbf{i}_n, \theta_o, \phi_o)$) differs from the power density for gain (i.e., $U(\mathbf{i}_1, \theta_o, \phi_o)$). In addition, the radiation efficiency, defined as the maximum gain divided by the maximum directivity, is represented by the following equation:

$$\eta \triangleq \frac{G}{D} = \frac{U_{\max}(\mathbf{i}_1, \theta_o, \phi_o) P_r}{U_{\max}(\mathbf{i}_n, \theta_o, \phi_o) P_{in}} \quad (25)$$

which incorporates the maximum radiation density for the lossless case (i.e., $U_{\max}(\mathbf{i}_n, \theta_o, \phi_o)$) and the lossy case (i.e., $U_{\max}(\mathbf{i}_1, \theta_o, \phi_o)$).

It is noted that in the literature, the radiation efficiency is often defined as the ratio of the radiated power to the input power, expressed as

$$\eta = \frac{P_r}{P_{in}}. \quad (26)$$

Equation (26) follows from (25), assuming an identical power density in both directivity and gain estimation. However, it is crucial to note that power density depends on the input currents, which vary when estimating directivity and gain. The input currents account for ohmic losses in the gain estimation, but this consideration is absent in the directivity estimation. Consequently, this disparity leads to inaccuracies when using (26) to calculate radiation efficiency. For instance, when considering the scenario where copper wires with lengths $L_1 = L_2 = \lambda/2$, radii $a_1 = a_2 = \lambda/1001$, are placed side by side at a distance $d = \lambda/2$, and driven by voltages $V_1 = V_2 = 1$ V, the calculated value of η based on (25) is 99%. On the other hand, applying (26) yields a different value of 100.94%, clearly demonstrating the inaccuracies caused by the application of this simplified formula.

Another important parameter is the realized gain, which is defined as the product of the port efficiency η_{port} and the gain, and thus

$$G_R \triangleq \eta_{port} G \quad (27)$$

where

$$\eta_{port} = 1 - |\Gamma_a|^2 = \frac{\mathbf{v}^H (\mathbf{I} - \mathbf{S}^H \mathbf{S}) \mathbf{v}}{\mathbf{v}^H \mathbf{v}} \quad (28)$$

where Γ_a is the total active reflection coefficient [31], [32], \mathbf{S} is the S -parameter matrix of the two-port network, calculated at the reference impedance of $Z_0 = 50 \Omega$, and \mathbf{I} is an identity matrix with the same dimension as \mathbf{S} .

The antenna array was optimized to achieve superdirectivity. The goal was to maximize the directivity, gain (which considers ohmic losses, equivalently radiation efficiency), and realized gain (which accounts for both radiation efficiency and return losses at 50Ω in our case) by varying the interelement

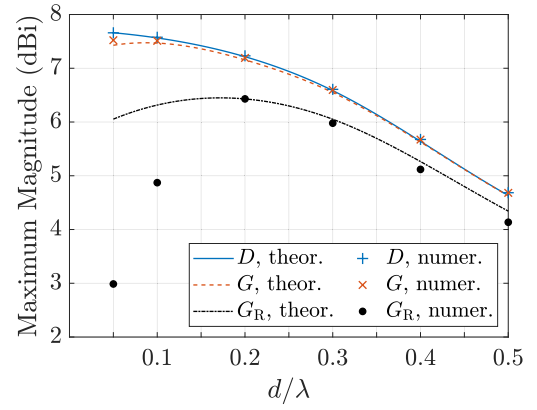


Fig. 2. Endfire directivity, gain, and realized gain of the optimal antenna array in terms of dB scaling are analyzed in relation to the interelement distance (analytical and numerical results).

distance from 0.1λ to 0.5λ , where λ is the operating wavelength (assumed to be 3.5 GHz for sub-6 GHz 5G systems). The analysis is based on theoretical calculations and formulas, i.e., on (15), (19), and (27). Design parameters include the lengths (L_1, L_2), radii (a_1, a_2), and interelement phase difference ($\Delta\phi$). In contrast to the state-of-the-art approach [9], [14], [15], [16], we fixed the driven voltages' magnitude at 1 V/m to avoid using additional components such as amplifiers or attenuators.

Particle swarm optimization (PSO) was used as the optimization method for the solution of the problem

$$\begin{aligned} &\text{Maximize}_{\{L_1, L_2, a_1, a_2, \Delta\phi\}} f(L_1, L_2, a_1, a_2, \Delta\phi) \\ &\text{subj. to: } L_1, L_2 \in [0.4\lambda, 0.6\lambda] \\ &\quad a_1, a_2 \in [\lambda/2001, \lambda/201] \\ &\quad \Delta\phi \in [0^\circ, 360^\circ] \end{aligned} \quad (29)$$

where function f represents the directivity (15), the gain (19), or the realized gain (27). Each interelement distance had an optimal set of design parameters for maximum directivity, gain, and realized gain. The results in Fig. 2 reveal a significant increase in directivity as the interelement distance approaches zero, indicating superdirectivity. The gain reaches its maximum when the interelement distance is approximately 0.1λ , accounting for ohmic losses. Similarly, the realized gain, which considers return losses at 50Ω , peaks at an interelement distance of around 0.2λ (specifically at 0.17λ). In contrast, the directivity trend alone suggests enhancement as d tends to zero with appropriate excitation signals, and this finding does not account for ohmic losses or return losses. Moreover, the directivity calculated at $d = 0.2\lambda$ is 7.3 dBi. In addition, the directivity estimated in [9] for two isotropic elements is 3.5 when using linear scaling. In our specific scenario, considering dipoles of length close to half-wavelength and a theoretical maximum directivity of 1.67, the predicted directivity is $10 \log_{10}(1.67 \cdot 3.5) \approx 7.7$ dBi, which closely aligns with our findings.

Fig. 3 depicts the optimal interelement phase difference ($\Delta\phi$) for achieving maximum directivity, gain, and realized gain as a function of interelement distance. While $\Delta\phi$ displays significant variation for realized gain, it remains approximately 200° for directivity and gain, even up to an interelement distance of 0.4λ . This observation suggests that the directivity and gain are relatively insensitive to phase setting.

TABLE I
OPTIMUM DESIGN PARAMETERS: THEORETICAL ANALYSIS AT 3.5 GHz

d/λ	L_1/λ	L_2/λ	a_1/λ	a_2/λ	$\Delta\phi$ (deg.)	η_{port}	η (%)	G_R (dBi)
0.05	0.480	0.482	0.0050	0.005	345.8°	0.763	94.2	6.1
0.1	0.473	0.467	0.0050	0.005	320.8°	0.807	98.4	6.3
0.2	0.479	0.452	0.0015	0.002	239.3°	0.925	98.8	6.4
0.3	0.474	0.437	0.0009	0.005	208.5°	0.978	99.2	6.1
0.4	0.466	0.440	0.0012	0.005	193.5°	0.997	99.5	5.3
0.5	0.448	0.448	0.0050	0.005	180°	0.987	99.8	4.3

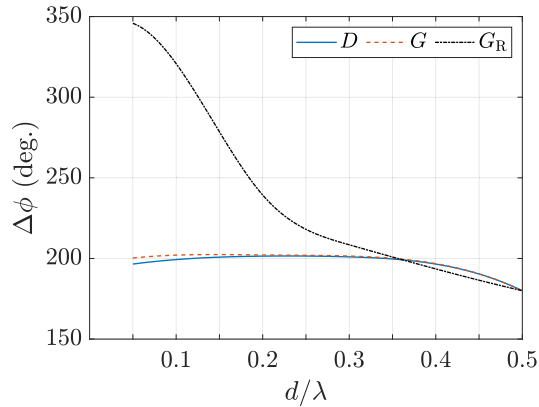


Fig. 3. Interelement phase difference for maximum endfire directivity, gain, and realized gain of a two-wire dipole antenna array versus interelement distance. The remaining design parameters (i.e., L_1 , L_2 , a_1 , and a_2) are held constant at their optimal values.

Finally, Table I provides insight into the lengths (L_1 , L_2) and radii (a_1 , a_2) yielding the maximum realized gain as a function of the interelement distance. Notably, the lengths of the wire dipoles consistently remain below half-wavelength for interelement distances up to 0.5λ . This suggests that optimizing the lengths within this range is crucial for achieving high realized gain. In addition, the radii of the wire dipoles appear to approach the upper limit of $\lambda/201 \approx 0.005\lambda$ in most cases. This observation implies that increasing the radius of the wires may lead to even higher realized gain. However, to maintain the assumption of a valid sinusoidal current distribution over the dipoles, we adhered to the empirical rule of keeping the wires as thin as possible.

According to Harrington's study [6], the maximum directivity, D_{max} , of a lossless antenna that completely fills a sphere with radius a is given by the equation

$$D_{max} = (ka)^2 + 2ka \quad (30)$$

where $k = 2\pi/\lambda$ is the wavenumber. The term ka is also known as the antenna's *electrical size*. In our specific case, with an interelement distance of 0.2λ , the resulting radius a is approximately 22 mm. Applying Harrington's findings, the maximum directivity of such an antenna is 7.7 dBi, which aligns with our expectations. In addition, the achieved realized gain reaches a maximum of 6.4 dBi, indicating close proximity to this theoretical upper limit.

These analytical findings suggest that it is feasible to implement a practical super realized gain antenna by carefully designing the dipoles in the array.

B. Numerical Analysis

Concluding the theoretical analysis presented in the previous section, we validated our findings through numerical analysis. Specifically, we first applied the method of moments using the Antenna Toolbox of MATLAB [33]. We modeled the dipoles using the *dipoleCylindrical* function and the array using the *linearArray* function. The conductor was defined using the *metal* function, with a conductivity of 5.8×10^7 S/m and a thickness of 35 μm . We used the same optimum design parameters as in the theoretical study. The results are depicted in Fig. 2. Regarding the directivity, there is a perfect agreement between the theoretical and numerical results from 0.05λ to 0.5λ . A good agreement is also observed for the gain case. However, as the dipoles get closer to each other or become thicker, the agreement for the realized gain decreases. This has an impact on the estimation of (21), which in turn affects the resulting impedance matrix \mathbf{Z}_i in (22). The impedance matrix is used to calculate the S -parameters in (28). Note that the numerical method estimates the current distribution on the surface of a cylinder with radius a_i , which differs from the linear distribution predicted in the theoretical analysis based on (4). Therefore, as the radius increases, the assumption of (4) becomes less accurate.

One of the main objectives of this work is to construct an SDA. Therefore, although wire dipoles offer analytical expressions and their theoretical study is feasible, we have chosen to focus on strip dipoles instead due to the advantages offered by the fabrication process. For example, fabricating wire dipoles with accurate interelement distance is challenging compared with the fabrication of strip dipoles with accurate widths. Strip dipoles can be easily manufactured by etching metal traces on PCB substrates, resulting in structurally robust configurations and accurate geometries. In addition, strip dipoles often exhibit a wider bandwidth compared with wire dipoles [30].

For comprehensive electromagnetic numerical simulations, we used the commercial solver CST Studio Suite 2022 [34], specifically the time-domain solver. This software allowed accurate modeling of the antenna array, analysis of its radiation pattern characteristics, and examination of the array's impedance. The simulated array is depicted in Fig. 4. Copper material with a conductivity of 5.96×10^7 S/m and a thickness of 35 μm was used for the metallic components. The strip dipoles were defined by their respective lengths, L_1 and L_2 , widths, w_1 and w_2 , and positioned at a distance of d from each other. The dipoles were driven by input voltages V_1 and V_2 . Discrete ports with 50 Ω were used to model the excitation of the array. For practical reasons, the strips were modeled on a substrate based on RO4003C, with a thickness of 0.813 mm,

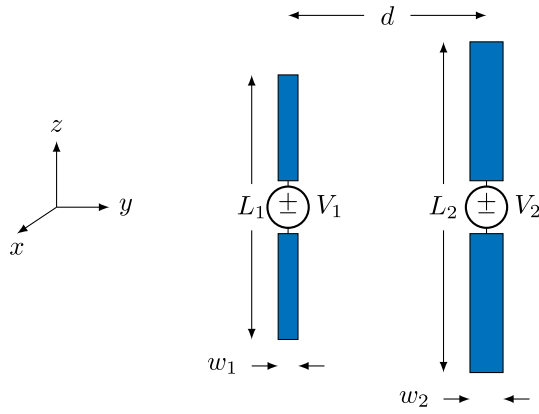


Fig. 4. Strip dipole array with interelement distance d , lengths and widths of elements L_1 and L_2 , and w_1 and w_2 , respectively, and excitation signal applied to the elements V_1 and V_2 .

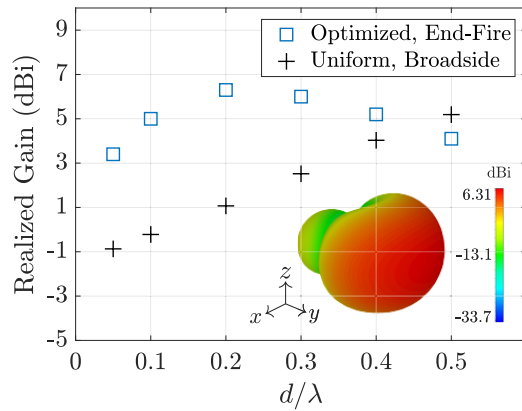


Fig. 5. Antenna array’s realized gain for the optimized and uniform cases versus interelement distance at 3.5 GHz (simulated results). The 3-D radiation pattern for the optimized result when $d = 0.2\lambda$ is also shown.

a dielectric constant of $\epsilon_r = 3.55$, and a dissipation factor of $\tan \delta = 0.0027$. The modeled substrate was assumed to have dimensions of 50×50 mm.

The antenna array was optimized to achieve superdirectivity by maximizing the realized gain while varying the interelement distance from 0.05λ to 0.5λ (at 3.5 GHz). The design parameters included the lengths L_1 and L_2 , the widths w_1 and w_2 , and the interelement phase difference $\Delta\phi \in [0, 360^\circ]$ of the elements. To keep implementation complexity low, the magnitude of the driven voltages was again fixed at 1 V/m.

The PSO method was used once again. The outcomes are shown in Fig. 5, which displays the maximum achieved antenna array realized gain as a function of the interelement distance d , maximized to 6.3 dBi at $d = 0.2\lambda$. It is evident that each d value has an optimal set of design parameters that yield the highest realized gain (Table II).

When considering the uniform case for $d = 0.2\lambda$, the array exhibits a realized gain of 1.1 dBi and is broadside. This indicates an improvement of approximately 5.2 dBi for the superdirective array.

In addition, for $d \geq \lambda/2$, the antenna array becomes broadside, and the improvement is marginal, as the optimized antenna realized gain only slightly differs from the uniform case. This aligns with expectations, as the superdirectivity phenomenon does not occur under these conditions (i.e., when $d \geq \lambda/2$).

TABLE II
OPTIMUM DESIGN PARAMETERS: NUMERICAL ANALYSIS
AT 3.5 GHz (STRIP DIPOLES ON SUBSTRATE)

d/λ	L_1 (mm)	L_2 (mm)	w_1 (mm)	w_2 (mm)	$\Delta\phi$ (deg.)	η (%)	G_R (dBi)
0.05	36.23	28.89	2.05	3.18	256°	99.2	3.4
0.1	42.39	30.39	4.85	3.19	210°	99.5	5.0
0.2	34.27	29.48	4.40	3.19	214°	99.3	6.3
0.3	33.33	29.62	5.14	2.57	197°	99.5	6.0
0.4	31.47	29.83	5.31	3.28	196°	99.6	5.2
0.5	30.74	29.77	4.14	3.24	172°	99.7	4.1

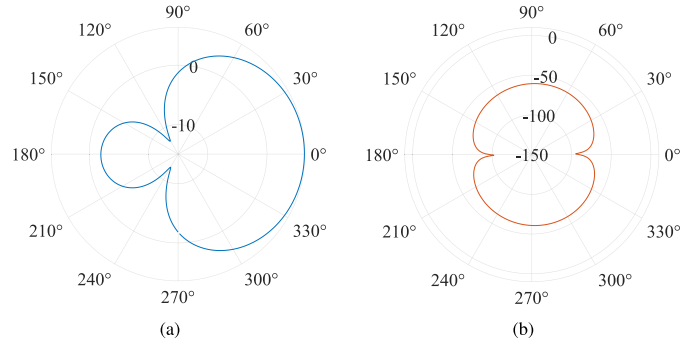


Fig. 6. Simulated realized gain radiation patterns in the horizontal plane (xy plane) for (a) co-polar pattern where maximum realized gain is achieved at $\phi = 0^\circ$, and for (b) cross-polar pattern, which is significantly less, denoting the antenna’s strong linear polarization.

The radiation efficiency η as a function of d/λ is also listed in Table II for interelement distances up to 0.5λ . It can be observed that the antenna array exhibits extremely high radiation efficiency, exceeding 99.2% for all interelement cases computed.

Fig. 6 illustrates the simulated realized gain in the horizontal plane (xy plane) for the optimal case with an element spacing of $d = 0.2\lambda$. The maximum simulated realized gain achieved is 6.3 dBi, observed at $\phi = 0^\circ$ in the co-polar plot, indicating an endfire antenna array configuration. The angular width, estimated at the 3 dB drop-off points, is 126° . Fig. 6 also illustrates the cross-polarized realized gain in the horizontal plane, highlighting the linear polarization of the antenna.

In SDAs, the surface current distribution plays a crucial role in achieving high directivity and gain [30], and it is typically nonuniform. It is characterized by strong currents flowing in specific regions of the array elements while minimizing currents in other areas. This nonuniform current distribution helps in shaping the radiation pattern and achieving high directivity. The specific current distribution pattern depends on the design and geometry of the array elements. The spacing, size, and arrangement of the elements, as well as the excitation amplitudes and phases, all contribute to the desired surface current distribution. In this work, the simulated surface current distribution is depicted in Fig. 7. It is evident that the distribution is not uniform, as expected.

The impact of the phase difference $\Delta\phi$ on the realized gain, with all other design parameters at their optimal values, is depicted in Fig. 8. The graph demonstrates that varying the phase difference to 175° or 253° from the maximum at 215° leads to a reduction in realized gain of 0.5 dB. This observation

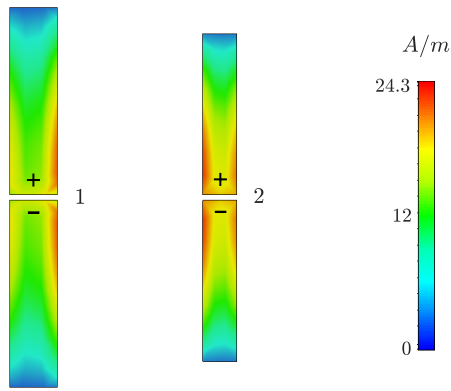


Fig. 7. Simulated surface current distribution for simultaneous optimal excitation at 3.5 GHz, when the interelement distance is 0.2λ . Ports are numbered, and strip dipoles lie on an RO4003C substrate.

is of significance in fabrication, as minor deviations in the phase difference do not exert a substantial influence on the maximum realized gain.

C. Implementation and Measurements

After completing the theoretical study and conducting a comprehensive numerical analysis using full-electromagnetic simulation, we proceed to the implementation phase. The antenna array is fabricated based on the design concept discussed above, which involves strip dipoles with slightly different lengths and radii (or widths). These dipoles are excited by signals of equal magnitude but different phases, enabling impedance-matching to 50Ω .

For validation purposes, the antenna array with an interelement distance of $d = 0.2\lambda$ was selected. To achieve a precise phase difference, coaxial cables (RG405) of different lengths were used to feed the strip dipoles. The strips were etched on an RO4003C substrate with a thickness of 0.813 mm, a dielectric constant of $\epsilon_r = 3.55$, and a dissipation factor of $\tan \delta = 0.0027$. A balun (balanced to unbalanced) of length $\lambda/4$ was incorporated to match the balanced structure of the dipole with the unbalanced structure of the coaxial cable, as shown in Fig. 9. SMA connectors were used for feeding. Before fabrication and measurement, the antenna array was subjected to numerical simulation to determine the optimal design parameters. Similar to the previous design, the lengths L_1 , L_2 , w_1 , and w_2 were considered. However, this time, to achieve the optimal phase difference, the length of the first coaxial cable (L_{c1}) was fixed at $L_{c1} = \lambda/2$ and the optimal length of the second cable (L_{c2}) was determined. Following numerical optimization, the final design parameters were obtained: $L_1 = 33.7$ mm, $L_2 = 29.1$ mm, $w_1 = 4.8$ mm, $w_2 = 3.5$ mm, and $L_{c2} = 81.3$ mm.

To measure the realized gain, we used the method of three antennas [30]. This method involves the use of a transmitting antenna (Tx), the antenna under test (AUT), and a reference antenna. In our setup, we opt to use identical transmitting and reference antennas [35] to simplify calculations. A signal generator was used at the transmitter, emitting at a frequency of 3.5 GHz with a power of 0 dBm, while a vector network analyzer (VNA) was used at the receiver. In addition, we took into account any losses incurred by the cables used in our setup. Instead of using a power divider, we performed our

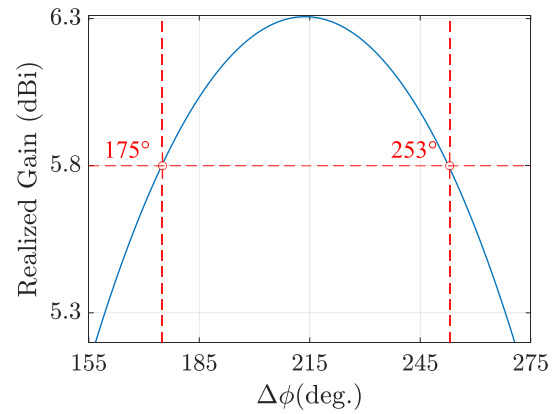


Fig. 8. Impact of the phase difference $\Delta\phi$ on the realized gain (simulated results): when $\Delta\phi$ ranges from 175° to 253° , the realized gain experiences a decrease of merely 0.5 dB.

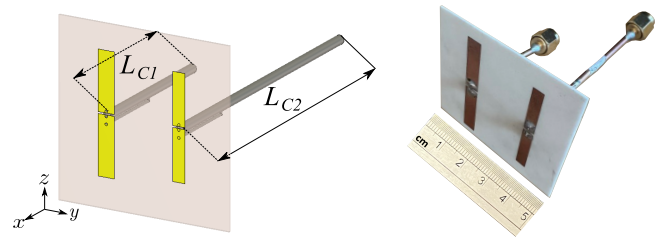


Fig. 9. (Left) Prior to fabrication, the antenna array underwent simulation to obtain optimal values for the design parameters. In this scenario, the interelement phase difference was achieved using coaxial cables of different lengths: L_{c1} was fixed at $\lambda/2$, while L_{c2} was estimated as a design parameter instead of $\Delta\phi$. In addition, a Pawsey balun with a length of $\lambda/4$ was implemented on both the dipoles to ensure a smooth transition from the coaxial cables to the strip dipoles. (Right) Fabricated antenna array.

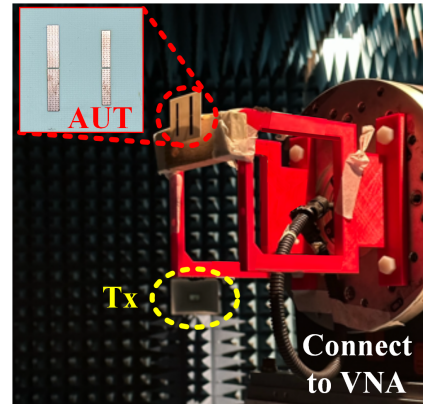


Fig. 10. Measurement setup in anechoic chamber and the AUT.

measurement in two steps and then combined the results algebraically. Specifically, in the first step, we measured the received power at the first dipole while terminating the second dipole at 50Ω . In the second step, we repeated the process but with the roles of the first and second dipoles reversed. The AUT was rotated to obtain the received power in the horizontal plane (H-plane). Due to the antenna's symmetry, we measured the rotation angles from 0° to 180° . All the measurements were conducted within the controlled environment of an anechoic chamber, as shown in Fig. 10.

The measured results, along with the simulated results, are shown in Fig. 11. Good agreement is observed between

TABLE III
COMPARISON OF TWO-ELEMENT SDAS

Reference	Element Type	f_c (GHz)	ka	D_{\max} (dBi)	D (dBi)	G or η	G_R (dBi)	Impedance Matched at 50 Ω	Complexity*
[9]	Wire Monopole	0.4	7.11	18.1	N/P	9.5 dBi	N/P	No	High
[12]	Magnetic Dipole	0.435	3.28	12.4	9.9	7.3 dBi, 55%	N/P	Yes (Parasitic element)	High
[22]	Planar Monopole	5.3	47.13	33.6	8.3	80.0%	N/P	Yes (Load element)	Moderate
[23]	Folded Dipole	0.878	N/P	N/P	7.0	6.8 dBi	N/P	N/P	Moderate
[24]	Printed Half-loop	0.901	1.22	6	6.8	70%	N/P	Yes (Parasitic/Load elements)	Moderate
Proposed Antenna	Strip Dipole	3.5	1.55	7.4	6.5	6.47 dBi, 99.3%	6.3	Yes	Low

* We have assumed that the use of amplifiers, attenuators and/or extra impedance matching network consist high-complexity, the use of load and/or parasitic elements moderate-complexity and none of these low-complexity. N/P: Not Provided, ka : antenna's electrical size.

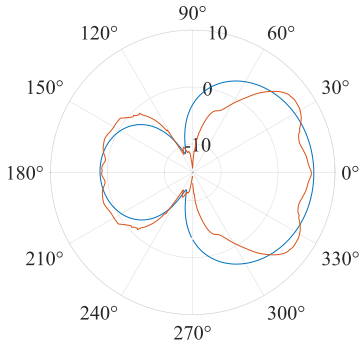


Fig. 11. Measured and simulated results of the realized gain in the horizontal plane (H-plane): indicating that the proposed antenna is behaving as a super realized gain antenna array, with a maximum realized gain of 6.3 dBi, at 3.5 GHz.

the measured and simulated results. At 3.5 GHz, the proposed antenna exhibits a measured realized gain of 6.3 dBi. The observed ripples could be due to balun manufacturing tolerances, the finite size of the substrate, or attenuation. Fig. 12 shows the measured and simulated S-parameters of the antenna array, demonstrating a high level of agreement between them. Furthermore, at 3.5 GHz, both S_{11} and S_{22} exhibit values below -10 dB, indicating low return losses at 50 Ω . The antenna operates within the frequency range of 3.44–3.62 GHz, resulting in a measured fractional bandwidth of 5.1%. In addition, by analyzing the S-parameters, we can estimate the impedance of each antenna element [30]. Specifically, the measured S-parameters at 3.5 GHz are presented in polar form (dB scale) as follows:

$$S = \begin{bmatrix} -14.5 / 19.2^\circ & -9.7 / 172.3^\circ \\ -9.8 / 172.3^\circ & -11.2 / 13.3^\circ \end{bmatrix}. \quad (31)$$

Thus, the measured antenna impedances at 3.5 GHz for the first $Z_{a,1}$ and second $Z_{a,2}$ radiating elements through the corresponding impedance parameters z are

$$Z_{a,1} = Z_{11} - \frac{Z_{12}Z_{21}}{Z_{22} + 50} = 70.9 + j9.1 \Omega \quad (32)$$

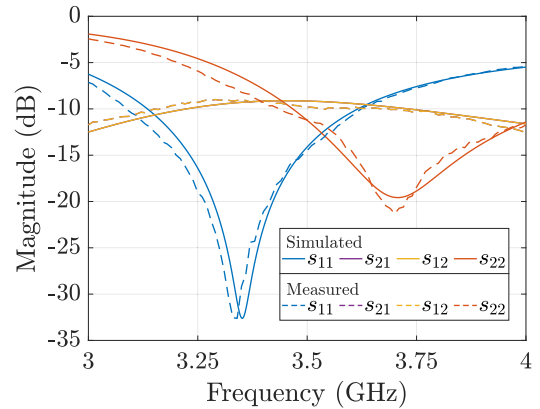


Fig. 12. Measured and simulated S-parameters of the fabricated antenna array. It is evident that the reflection coefficient of both the dipoles is less than -10 dB, indicating an impedance-matching to 50 Ω at the operating frequency of 3.5 GHz.

and

$$Z_{a,2} = Z_{22} - \frac{Z_{12}Z_{21}}{Z_{11} + 50} = 85.6 + j11.8 \Omega. \quad (33)$$

This results in reflection coefficients of -14.5 and -11.2 dB, respectively, which agree with the plot in Fig. 12. Thus, the measurements closely correspond with our theoretical and simulated results.

III. DISCUSSION

Table III provides a detailed comparative analysis of our proposed two-element superdirective antenna design against state-of-the-art alternatives. This analysis is based on prototype measurements at their operational frequencies, f_c . The comparison focuses on key performance metrics such as antenna directivity (D) and either gain (G) or radiation efficiency (η), which are critical attributes for antennas. In addition, we have calculated the maximum directivity (D_{\max}) in relation to Harrington's limit. Although this limit does not directly indicate superdirective behavior, it offers valuable insight into

how superdirectivity can lead to the development of highly directive antennas without increasing the antenna size. The table also includes a comparison of the antennas' realized gain, reflecting the efficiency of impedance-matching at 50Ω , a crucial aspect of our design methodology. The complexity of superdirective antenna designs is another focus area, acknowledging that implementing superdirectivity typically involves sophisticated features such as amplifiers, attenuators, parasitic elements, lumped loads, and impedance-matching networks. Conversely, a low-complexity design omits these elements, thereby simplifying the development approach.

In the work by Altschuler et al. [9], the experimental focus was on measuring of the gain of a two-element resonant monopole array across various spacings. The objective was to achieve superdirectivity by adjusting the magnitude and phase of the input signals to the monopoles. The experiments revealed a gain increase as the element spacing decreased, up until the point where the ohmic losses of the copper monopoles began to offset the gains. This research offers valuable insights into the practical challenges and limitations of SDAs, as it used attenuators and amplifiers to fine-tune the magnitude and phases of the driven monopoles. A gain of 9.5 dBi was achieved at an interelement distance of 0.2λ . While this is significantly higher than the gain achieved with uniform excitation, thereby justifying superdirective operation, it falls short of the maximum Harrington's limit of 18.1 dBi when considering the size of the antenna's ground plane.

The research presented in [12] explores the design of a superdirective antenna. This design uses a slot magnetic dipole as the radiator and two other magnetic dipoles as parasitic elements. The prototype effectively demonstrated that the antenna's directivity could be increased using a single active element, complemented by passive elements arranged in a Yagi-Uda configuration. The antenna operates on a metal ground plane and exhibits a maximum measured directivity of $D = 9.9$ dBi at a frequency of 435 MHz. When considering the total size of the antenna, the maximum directivity, according to Harrington's method, is $D_{max} = 12.4$ dBi. Another notable aspect of this antenna is its measured gain of $G = 7.3$ dBi, which results in a radiation efficiency of only 55%.

In the work by Mazinani and Hassani [22], a new approach is explored to boost the directivity of a two-element planar monopole antenna array by attaching small parallel plates to the monopoles' radiating edges and finely tuning the elements' spacing and relative phase shift between the elements. The research resulted in enhanced directivity, recording a maximum of $D = 8.3$ dBi at 5.3 GHz and a radiation efficiency of 80%. Despite these improvements, the maximum directivity remains significantly below the theoretical limit of $D_{max} = 33.6$ dBi, as dictated by Harrington's bound, which considers the antenna's total dimensions, including the ground plane.

The study in [23] investigates the theoretical limits and experimental validation of SDAs. The research is centered on deriving the upper bounds for the directivity of linear arrays, constructed from closely spaced radiating elements, specifically electrical dipoles. This is achieved using a spherical wave expansion (SWE) as a function of the number of array elements and their interelement spacing. The researchers proposed a new bound for the maximum achieved directivity,

which differs from Harrington's limit. The theoretical findings were validated through the experimental testing of three array configurations, each with two, three, and four elements. In all the antenna configurations, a single folded element is driven using a balun, complemented by passive strip dipole elements arranged in a Yagi-Uda configuration. These elements are loaded with resistance and inductance components. For the four-element array (a folded dipole is driven, and the remaining three elements are strip passive dipoles), the proposed theoretical method predicts a maximum directivity of 12.4 dBi at 0.850 GHz. This aligns well with the simulated figure of 12.2 dBi. The measurements for the directivity were conducted at a slightly different frequency of 0.852 GHz and showed a maximum of 10.3 dBi. The corresponding values for the gain are -1.7 (theoretical), -1.1 (simulated), and 2.1 (measured) dBi, respectively, resulting in a measured radiation efficiency of only 15%. To increase the antenna gain from -1.7 to 2.1 dBi, the parasitic dipoles were loaded with connected resistance and inductance components. For the two-element array, the proposed theoretical model predicted a maximum theoretical directivity and gain of $D = 7$ dBi and $G = 5.9$ dBi, respectively, resulting in a radiation efficiency of 77.6% at 0.85 GHz. To increase the measured gain, a load component is again connected to the parasitic element, and then the maximum measured gain was $G = 6.8$ GHz, but at a different frequency of 0.878 GHz. Although the use of extra loads led to the enhancement of gain, the calculation of their values, which is discussed in detail in [26], and their difference with the commercially used loads, makes the antenna design challenging. In addition, for this work, the directivity based on Harrington's limit was not calculated and shown in Table III, as the exact size of the antennas was not mentioned. Finally, the impedance-matching properties of the antenna designs are not provided in this study, and hence not included in Table III.

The work presented in [24] introduces a method for designing parasitic coplanar, loaded SDAs. The study explores different antenna array geometries with a focus on achieving high directivity within compact designs. The research resulted in the creation and testing of a two-element prototype with a total size of $\lambda/3 \times \lambda/5$. The antenna resonated at 0.9 GHz and demonstrated a maximum measured directivity of $D = 6.8$ dBi. This signifies an increase in directivity of 0.8 dB over Harrington's limit, which is $D_{max} = 6$ dBi. However, the measured radiation efficiency was approximately $\eta = 70\%$. This indicates a tradeoff in the design between achieving superdirective performance and maintaining high radiation efficiency. The latter cannot be addressed merely using substrates of low losses, as the same research group mentioned in [25].

While the use of a matching network and a low-loss substrate can improve the antenna radiation efficiency (especially in grounded microstrip or printed antennas, where the substrate can introduce ohmic losses [36]), several other factors also play a crucial role, such as the antenna design approach [37], [38], [39]. In an antenna array of metallic strip dipoles lying on a substrate, the ohmic losses, which impact the antenna's radiation efficiency, primarily originate from the conductivity of the metallic parts of the antenna rather than from the dielectric losses of the substrate, due to the absence of a ground plane. This is mathematically expressed in (17)

and (21). In addition, the use of any load or parasitic element to achieve impedance-matching can increase the ohmic losses, thus reducing the radiation efficiency. In stark contrast to the state of the art, our antenna design approach for impedance-matched superdirective antennas does not include any loads or parasitic elements. This is the key factor in maintaining low ohmic losses and high radiation efficiency in our proposed superdirective antenna.

IV. CONCLUSION

Achieving superdirectivity in antenna arrays while maintaining high radiation efficiency and low impedance-matching losses remains a formidable challenge in the field of antenna design. Reviewing state-of-the-art methodologies reveals that substantial advancements have been made using parasitic elements, often complemented with loading to enhance directivity and decrease the impedance-matching losses. However, this approach frequently results in reduced radiation efficiency and necessitates complex antenna designs to balance performance metrics. Particularly, when using low-profile elements such as monopoles, the integration of attenuators and even amplifiers becomes essential, further complicating the design process. Moreover, the incorporation of ground planes, although beneficial for certain antenna properties, tends to increase the overall size of the antenna system without proportionately enhancing maximum directivity. This often results in a significant disparity between achieved directivity and the theoretical Harrington's limit. Contrasting these challenges, our method introduces a novel design of a low-profile, super realized gain antenna, using merely strip dipoles with subtle variations in length and width. This approach simplifies the design process not only by avoiding the need for parasitic elements, extensive ground planes, and loads but also effectively bridges the gap between practical directivity achievements and theoretical limits, marking a significant leap forward in superdirective antenna array design.

REFERENCES

- [1] S. D. Assimonis, M. A. B. Abbasi, and V. Fusco, "Millimeter-wave multi-mode circular antenna array for uni-cast multi-cast and OAM communication," *Sci. Rep.*, vol. 11, no. 1, p. 4928, Mar. 2021.
- [2] K. Hu, T. W. Callis, and M. M. Tentzeris, "Additively manufactured flexible on-package phased antenna arrays with integrated microfluidic cooling channels for 5G/mmWave system-on-package designs," *IEEE Microw. Wireless Technol. Lett.*, vol. 33, no. 6, pp. 899–902, Jun. 2023.
- [3] A. Eid, J. G. D. Hester, and M. M. Tentzeris, "5G as a wireless power grid," *Sci. Rep.*, vol. 11, no. 1, p. 636, Jan. 2021.
- [4] A. I. Uzkov, "An approach to the problem of optimum directive antenna design," *Comp. Rendus (Doklady) de l'Academie des Sci. de l'URSS*, vol. 53, pp. 35–38, Jun. 1946.
- [5] R. C. Hansen, "Fundamental limitations in antennas," *Proc. IEEE*, vol. 69, no. 2, pp. 170–182, Feb. 1981.
- [6] R. Harrington, "On the gain and beamwidth of directional antennas," *IRE Trans. Antennas Propag.*, vol. 6, no. 3, pp. 219–225, Jul. 1958.
- [7] N. Yaru, "A note on super-gain antenna arrays," *Proc. IRE*, vol. 39, no. 9, pp. 1081–1085, Sep. 1951.
- [8] M. Uzsoy and L. Solymár, "Theory of super-directive linear arrays," *Acta Phys. Academiae Scientiarum Hungaricae*, vol. 6, no. 2, pp. 185–205, Dec. 1956.
- [9] E. E. Altshuler, T. H. O'Donnell, A. D. Yaghjian, and S. R. Best, "A monopole superdirective array," *IEEE Trans. Antennas Propag.*, vol. 53, no. 8, pp. 2653–2661, Aug. 2005.
- [10] M. L. Morris, M. A. Jensen, and J. W. Wallace, "Superdirectivity in MIMO systems," *IEEE Trans. Antennas Propag.*, vol. 53, no. 9, pp. 2850–2857, Sep. 2005.
- [11] M. T. Ivrlač and J. A. Nossek, "High-efficiency super-gain antenna arrays," in *Proc. ITG Int. Workshop Smart Antennas*, Feb. 2010, pp. 369–374.
- [12] O. S. Kim, S. Pivnenko, and O. Breinbjerg, "Superdirective magnetic dipole array as a first-order probe for spherical near-field antenna measurements," *IEEE Trans. Antennas Propag.*, vol. 60, no. 10, pp. 4670–4676, Oct. 2012.
- [13] T. L. Marzetta, "Super-directive antenna arrays: Fundamentals and new perspectives," in *Proc. 53rd Asilomar Conf. Signals, Syst., Comput.*, Nov. 2019, pp. 1–4.
- [14] K. Dovelos, S. D. Assimonis, H. Q. Ngo, and M. Matthaiou, "Superdirective arrays with finite-length dipoles: Modeling and new perspectives," in *Proc. IEEE Global Commun. Conf. (GLOBECOM)*, Dec. 2022, pp. 6517–6522.
- [15] L. Han, H. Yin, and T. L. Marzetta, "Coupling matrix-based beamforming for superdirective antenna arrays," in *Proc. IEEE Int. Conf. Commun. (ICC)*, May 2022, pp. 5159–5164.
- [16] K. Dovelos, S. D. Assimonis, H. Q. Ngo, and M. Matthaiou, "Superdirective antenna pairs for energy-efficient terahertz massive MIMO," 2022, *arXiv:2207.00697*.
- [17] L. Han, H. Yin, M. Gao, and J. Xie, "A superdirective beamforming approach with impedance coupling and field coupling for compact antenna arrays," 2023, *arXiv:2302.08203*.
- [18] A. Tornese, A. Clemente, and C. Delaveaud, "A new method for gain prediction of superdirective end-fire arrays," in *Proc. 16th Eur. Conf. Antennas Propag. (EuCAP)*, Mar. 2022, pp. 1–4.
- [19] R. W. Ziolkowski, "Superdirective unidirectional mixed-multipole antennas: Designs, analysis, and simulations," *IEEE Trans. Antennas Propag.*, vol. 71, no. 7, pp. 5566–5581, Jul. 2023.
- [20] S. D. Assimonis, "How challenging is it to design a practical superdirective antenna array?" in *Proc. IEEE SENSORS*, Vienna, Austria, Oct. 2023, pp. 1–4.
- [21] B. Couraud et al., "Internet of Things: A review on theory based impedance matching techniques for energy efficient RF systems," *J. Low Power Electron. Appl.*, vol. 11, no. 2, p. 16, Mar. 2021, doi: [10.3390/jlpea11020016](https://doi.org/10.3390/jlpea11020016).
- [22] S. M. Mazinani and H. R. Hassani, "Superdirective wideband array of planar monopole antenna with loading plates," *IEEE Antennas Wireless Propag. Lett.*, vol. 9, pp. 978–981, 2010.
- [23] A. Debar, A. Clemente, A. Tornese, and C. Delaveaud, "On the maximum end-fire directivity of compact antenna arrays based on electrical dipoles and Huygens sources," *IEEE Trans. Antennas Propag.*, vol. 71, no. 1, pp. 299–308, Jan. 2023.
- [24] A. Haskou, A. Sharaiha, and S. Collardey, "Design of small parasitic loaded superdirective end-fire antenna arrays," *IEEE Trans. Antennas Propag.*, vol. 63, no. 12, pp. 5456–5464, Dec. 2015.
- [25] A. Haskou, A. Sharaiha, and S. Collardey, "Integrating superdirective electrically small antenna arrays in PCBs," *IEEE Antennas Wireless Propag. Lett.*, vol. 15, pp. 24–27, 2016.
- [26] A. Clemente, M. Pigeon, L. Rudant, and C. Delaveaud, "Design of a super directive four-element compact antenna array using spherical wave expansion," *IEEE Trans. Antennas Propag.*, vol. 63, no. 11, pp. 4715–4722, Nov. 2015.
- [27] D. M. Pozar, *Microwave Engineering*, 4th ed., Hoboken, NJ, USA: Wiley, 2011.
- [28] S. J. Orfanidis. (2016). *Electromagnetic Waves and Antennas*. [Online]. Available: <http://eceweb1.rutgers.edu/~orfanidi/ewa/>
- [29] L. F. Shampine, "Vectorized adaptive quadrature in MATLAB," *J. Comput. Appl. Math.*, vol. 211, no. 2, pp. 131–140, Feb. 2008.
- [30] C. A. Balanis, *Antenna Theory: Analysis Design*. Hoboken, NJ, USA: Wiley, 2005.
- [31] M. Manteghi and Y. Rahmat-Samii, "Broadband characterization of the total active reflection coefficient of multiport antennas," in *IEEE Antennas Propag. Soc. Int. Symp. Dig.*, vol. 3, Jun. 2003, pp. 20–23.
- [32] S. Moradi, B. Honarbakhsh, and T. F. Eibert, "Some excitation independent bounds for the total active reflection coefficient of antenna arrays," *IEEE Trans. Antennas Propag.*, vol. 70, no. 12, pp. 11743–11751, Dec. 2022.
- [33] *MATLAB Version R2022b*, MathWorks, Natick, MA, USA, 2022.
- [34] Dassault Systemes. (2022). *CST Studio Suite*. [Online]. Available: <https://www.3ds.com/products-services/simulia/products/cst-studio-suite/>
- [35] SunAR RF Motion. (2023). *DRH Series Broadband Horn Antennas*. [Online]. Available: <https://www.sunarrfmotion.com/horn-antennas/>

- [36] T. Yousefi, T. Sebastian, and R. E. Diaz, "Why the magnetic loss tangent is not a relevant constraint for permeable conformal antennas," *IEEE Trans. Antennas Propag.*, vol. 64, no. 7, pp. 2784–2796, Jul. 2016.
- [37] C. Pfeiffer, "Fundamental efficiency limits for small metallic antennas," *IEEE Trans. Antennas Propag.*, vol. 65, no. 4, pp. 1642–1650, Apr. 2017.
- [38] C. Pfeiffer, "Upper bounds on the radiation efficiency of electrically small antennas," in *Proc. IEEE Int. Symp. Antennas Propag. USNC/URSI Nat. Radio Sci. Meeting*, Jul. 2017, pp. 1197–1198.
- [39] T. Nahar and S. Rawat, "Efficiency enhancement techniques of microwave and millimeter-wave antennas for 5G communication: A survey," *Trans. Emerg. Telecommun. Technol.*, vol. 33, no. 9, Sep. 2022, Art. no. e4530.



Dónal Patrick Lynch (Graduate Student Member, IEEE) received the B.S. degree in electrical and electronic engineering from Queen's University Belfast, Belfast, U.K., in 2021, where he is currently pursuing the Ph.D. degree with the Institute of Electronics, Communication and Information Technology (ECIT).

He has been actively involved in research projects that focus on the development of innovative antenna technologies, contributing to several publications in reputed journals and conferences. His research interests

include superdirective antenna arrays, electrically small antennas, and metasurface applications.



Manos M. Tentzeris (Fellow, IEEE) received the Diploma degree (magna cum laude) in electrical and computer engineering from the National Technical University of Athens, Athens, Greece, in 1992, and the M.S. and Ph.D. degrees in electrical engineering and computer science from the University of Michigan, Ann Arbor, MI, USA, in 1993 and 1998, respectively.

He was a Visiting Professor at the Technical University of Munich, Munich, Germany, in 2002; GTRI-Ireland, Athlone, Ireland, in 2009; LAAS-

CNRS, Toulouse, France, in 2010; and a Humboldt Guest Professor with FAU, Nuremberg, Germany, in 2019. He is currently the Ed and Pat Joy Chair Professor with the School of Electrical and Computer Engineering, Georgia Institute of Technology, Atlanta, GA, USA, where he heads the ATHENA Research Group (20 researchers). He has served as the Head of the GT ECE Electromagnetics Technical Interest Group, Georgia Electronic Design Center, Atlanta, GA, USA, the Associate Director of RFID/Sensors Research, Georgia Institute of Technology NSF-Packaging Research Center, an Associate Director of RF Research, and the RF Alliance Leader. He has helped develop academic programs in 3-D/inkjet-printed RF electronics and modules, flexible electronics, origami and morphing electromagnetics, highly integrated/multilayer packaging for RF, millimeter-wave, subterahertz, and wireless applications using ceramic and organic flexible materials, paper-based RFID's and sensors, wireless sensors and biosensors, wearable electronics, "Green" and transient electronics, energy harvesting and wireless power transfer, nanotechnology applications in RF, microwave MEMs, and SOP-integrated (UWB, multiband, mmW, and conformal) antennas. He has authored more than 850 papers in refereed journals and conference proceedings, seven books, and 26 book chapters. He has given more than 150 invited talks to various universities and companies all over the world.

Dr. Tentzeris is a member of the URSI-Commission D and the MTT-15 Committee, an Associate Member of EuMA, a fellow of the Electromagnetic Academy, and a member of the Technical Chamber of Greece. He was a recipient/co-recipient of the 2024 Georgia Tech Outstanding Achievement in Research Innovation Award, the 2024 IEEE International Microwave Symposium (IMS) Best Student Paper Award, the 2023 Proceedings of IEEE Best Paper Award, the 2022 Georgia Tech Outstanding Doctoral Thesis Advisor Award, the 2021 IEEE Antennas and Propagation Symposium (APS) Best Student Paper Award, the 2019 Humboldt Research Prize, the 2017 Georgia Institute of Technology Outstanding Achievement in Research Program Development Award, the 2016 Bell Labs Award Competition Third Prize, the 2015 IET Microwaves, Antennas, and Propagation Premium Award, the 2014 Georgia Institute of Technology ECE Distinguished Faculty

Achievement Award, the 2014 IEEE RFID-TA Best Student Paper Award, the 2013 IET Microwaves, Antennas, and Propagation Premium Award, the 2012 FiDiPro Award in Finland, the iCMG Architecture Award of Excellence, the 2010 IEEE Antennas and Propagation Society Piergiorgio L. E. Uslenghi Letters Prize Paper Award, the 2011 International Workshop on Structural Health Monitoring Best Student Paper Award, the 2010 Georgia Institute of Technology Senior Faculty Outstanding Undergraduate Research Mentor Award, the 2009 IEEE Transactions on Components and Packaging Technologies Best Paper Award, the 2009 E. T. S. Walton Award from the Irish Science Foundation, the 2007 IEEE AP-S Symposium Best Student Paper Award, the 2007 IEEE MTT-S IMS Third Best Student Paper Award, the 2007 ISAP Poster Presentation Award, the 2006 IEEE MTT-S Outstanding Young Engineer Award, the 2006 Asia-Pacific Microwave Conference Award, the 2004 IEEE TRANSACTIONS ON ADVANCED PACKAGING Commendable Paper Award, the 2003 NASA Godfrey "Art" Anzic Collaborative Distinguished Publication Award, the 2003 IBC International Educator of the Year Award, the 2003 IEEE CPMT Outstanding Young Engineer Award, the 2002 International Conference on Microwave and Millimeter-Wave Technology Best Paper Award, Beijing, China, the 2002 Georgia Institute of Technology-ECE Outstanding Junior Faculty Award, the 2001 ACES Conference Best Paper Award, the 2000 NSF CAREER Award, and the 1997 Best Paper Award of the International Hybrid Microelectronics and Packaging Society. He was the General Co-Chair for the 2023 IEEE Wireless Power Transfer Technology Conference and Expo (WPTCE) in San Diego and the 2019 IEEE APS Symposium in Atlanta. He was the TPC Chair for the IEEE MTT-S IMS 2008 Symposium and the Chair for the 2005 IEEE CEM-TD Workshop. He is the Vice-Chair for the RF Technical Committee (TC16) of the IEEE CPMT Society. He is the Founder and the Chair for the RFID Technical Committee (TC24) of the IEEE MTT-S and the Secretary/Treasurer of the IEEE C-RFID. He has served as an Associate Editor for IEEE TRANSACTIONS ON MICROWAVE THEORY AND TECHNIQUES, IEEE TRANSACTIONS ON ADVANCED PACKAGING, and the *International Journal on Antennas and Propagation*. He is currently the IEEE EPS Distinguished Lecturer and has served as one of the IEEE MTT-S Distinguished Microwave Lecturers and as one of the IEEE CRFID Distinguished Lecturers.



Vincent Fusco (Fellow, IEEE) specializes in microwave through submillimeter antennas and circuits. He holds 12 patents and has published more than 650 peer-reviewed research papers and two books. He is credited for his work on self-tracking antenna arrays.

Dr. Fusco is a fellow of the Royal Society, U.K. Royal Academy of Engineering, Member of the Royal Irish Academy, the Irish Academy of Engineering, and the Institution of Engineering Technology (IET), and is a Chartered Engineer.

He was awarded a CBE in 2023 for his services to Engineering and Science. In 2012, he was awarded the IET Senior Achievement Award the Mountbatten Medal and in 2019 The Royal Irish Academy Gold Medal for Engineering Sciences.



Stylianos D. Asimonis (Senior Member, IEEE) received the Diploma (five years) and Ph.D. degrees in electrical and computer engineering from Aristotle University of Thessaloniki, Thessaloniki, Greece, in 2005 and 2011, respectively.

Currently, he holds the position of a Lecturer with the School of Electronics, Electrical Engineering and Computer Science, Queen's University, Belfast, U.K. He has co-authored numerous research papers in the fields of electromagnetics and RF engineering. His primary research interests include electromagnetic periodic structures, RF energy harvesting, and antennas.

Dr. Asimonis was honored with the Post-Doctoral Scholarship for Excellence by the Research Committee of Aristotle University of Thessaloniki and by the Centre for Wireless Innovation (CWI) at Queen's University Belfast, in 2012 and 2016, respectively. He received the distinguished paper awards at prominent events, such as Metamaterials 2013, the 2014 IEEE RFID-TA, and the 2015 5th COST IC1301 Workshop. He serves as an Editor for the *Nature Scientific Reports* and the *MDPI Journal of Low Power Electronics and Applications*. From 2019 to 2021, he acted as a Guest Editor for the *MDPI Journal of Low Power Electronics and Applications* and the *MDPI Sensors*.